Journal of Crystal Growth 407 (2014) 6–10

Contents lists available at ScienceDirect

Journal of Crystal Growth

journal homepage: www.elsevier.com/locate/jcrysgro

Defect reduction of SiN_x embedded *m*-plane GaN grown by hydride vapor phase epitaxy

Seohwi Woo, Minho Kim, Byeongchan So, Geunho Yoo, Jongjin Jang, Kyuseung Lee, Okhyun Nam *

Advanced Photonics Research Center/LED Technology Center, Department of Nano-Optical Engineering, Korea Polytechnic University, Siheung 429-793, Gyeonggi, Republic of Korea

ARTICLE INFO

Article history:
Received 13 December 2013
Received in revised form
14 July 2014
Accepted 13 August 2014
Communicated by M. Weyers
Available online 3 September 2014

Keywords:
A3. HVPE
A1. *m*-Plane GaN
Nonpolar
SiN_x
Defect reduction

ABSTRACT

Nonpolar (1 0 −1 0) *m*-plane GaN has been grown on *m*-plane sapphire substrates by hydride vapor phase epitaxy (HVPE). We studied the defect reduction of *m*-GaN with embedded SiN_x interlayers deposited by ex-situ metal organic chemical vapor deposition (MOCVD). The full-width at half-maximum values of the X-ray rocking curves for *m*-GaN with embedded SiN_x along $[1\,1\,-2\,0]_{GaN}$ and $[0\,0\,0\,1]_{GaN}$ were reduced to 528 and 1427 arcs, respectively, as compared with the respective values of 947 and 3170 arcs, of *m*-GaN without SiN_x. Cross-section transmission electron microscopy revealed that the basal stacking fault density was decreased by approximately one order to $5 \times 10^4\ cm^{-1}$ due to the defect blocking of the embedded SiN_x. As a result, the near band edge emission intensities of the room-temperature and low-temperature photoluminescence showed approximately two-fold and four-fold improvement, respectively.

© 2014 Elsevier B.V. All rights reserved.

1. Introduction

Among Group III-nitride materials, GaN has been widely utilized for visible and ultraviolet light-emitting diodes and high-power electronic devices [1,2]. These devices, which are conventionally grown on the polar (0 0 0 1) plane, typically exhibit spontaneous and piezoelectric polarization effects, rendering them undesirable for many applications. The polarization effect causes band bending and reduces the radiative recombination efficiency in the quantum wells (QW), which, in turn, reduces the luminous efficiency of the devices due to the quantum-confined stark effect [3]. To eliminate this polarization effect, these devices should be grown on the semi-polar (1 1 −2 2) plane, the nonpolar (1 1 −2 0) *a*-plane GaN (*a*-GaN), or the nonpolar (1 0 −1 0) *m*-plane GaN (*m*-GaN). In particular, *m*-GaN is more stable and has a wider acceptable range of growth conditions compared with *a*-GaN [4]. Furthermore, *m*-GaN more readily accepts Mg, which enables p-type doping levels to be increased [5]. Consequently, using *m*-GaN in an optical device with a multi QW structure will help to improve the device performance. Because of these advantages, many research groups have reported heteroepitaxial *m*-GaN films grown on $LiAlO_2$ [6], *m*-plane SiC [7], patterned (1 1 2) Si [8], *m*-plane ZnO [9], and *m*-plane sapphire (*m*-sapphire) [10–12]. Among these, *m*-sapphire is the substrate of best choice for the growth of *m*-GaN because it is cost effective and larger substrate diameters are more readily available compared to $LiAlO_2$, SiC, or ZnO substrates. Moreover, *m*-sapphire is more chemically and thermally stable than either $LiAlO_2$ or ZnO. Thus, *m*-sapphire allows *m*-GaN growth without difficulty while protecting itself from an influx of impurities under high temperatures. In spite of these advantages, *m*-GaN grown directly on *m*-sapphire has a number of critical problems. In particular, high defect densities and an anisotropic crystal structure may occur because an antiphase domain boundary is formed from ambidirectional nucleation of *m*-GaN [13]. In order to solve this problem, the *m*-sapphire substrate was cut at an angle of 1° to 5° in the [11–20] direction [13]. As a result, the full-width at half-maximum (FWHM) was reduced in the double-crystal X-ray rocking curves (DXRCs) for *m*-GaN. The anisotropy was also reduced, though a minimal anisotropic DXRC FWHM value remained [13]. To avoid these problems, commercially available *m*-GaN substrates with a low defect density and high isotropic crystal quality were produced from small transverse slices of *c*-oriented bulk crystals grown by HVPE [14,15]. However, the small substrate size ($\sim a$ few mm^2), high substrate cost, and complicated process proved to be serious a drawbacks for industrial applications.

For these reasons, further studies are required to find a method that successfully prepares large-size *m*-GaN substrates with a low defect density and high isotropic crystal quality.

* Corresponding author.
E-mail address: ohnam@kpu.ac.kr (O. Nam).

http://dx.doi.org/10.1016/j.jcrysgro.2014.08.014
0022-0248/© 2014 Elsevier B.V. All rights reserved.

To solve this problem, several groups have reported an improvement in optical properties and defect reduction using SiN_x interlayers in *c*-GaN [16–18], *a*-GaN [19], and semi-polar (1 1 −2 2) GaN [21,22]. However, defect reduction using SiN_x interlayers has not yet been discussed for *m*-GaN.

In this study, we report, for the first time, an improvement in crystal quality and optical properties by reducing the defects in SiN_x embedded *m*-GaN grown on an *m*-sapphire substrate by HVPE. The reduced feature size of the SiN_x nanopores facilitates nanometer-scale epitaxial lateral overgrowth (ELO), which thereby results in uniform defect reduction in *m*-GaN on *m*-sapphire.

2. Experiments

The *m*-GaN samples were grown on *m*-sapphire substrates with a 2° miscut with respect to the *a*-axis using an atmospheric HVPE system. Using a vertical reactor heated by a two-zone furnace, the temperature of the substrate ranged from 900 to 1100 °C during growth. The source gases were NH_3 and GaCl (g) with the latter being formed by the reaction between Ga (s) and HCl(g). Nitrogen was used as a carrier gas. As shown in Fig. 1(a), an approximately 2-μm-thick layer of *m*-GaN was grown directly on *m*-sapphire by HVPE. Then, SiN_x was deposited on the HVPE *m*-GaN layer in the MOCVD system (close-coupled showerhead Thomas Swan reactor). During the SiN_x growth at 860 °C, the flow rate of NH_3 and SiH_4 was 8000 sccm and 45 sccm, respectively, and the growth time was 1500 s. Next, an approximately 2-μm-thick GaN layer was grown by MOCVD reactor, as shown in Fig. 1(b) and (c). Sub-monolayer SiN_x interlayer is randomly formed and functions as a defect-blocking layer. Finally, a 15-μm *m*-GaN layer was grown by HVPE, as shown in Fig. 1(d).

The surface and cross-section morphology of the *m*-GaN layers were observed by scanning electron microscopy (SEM) and atomic force microscope (AFM), while the crystal quality was determined by high-resolution X-ray diffraction (HRXRD) omega rocking curves.

The room-temperature (RT) and low-temperature (LT) photoluminescence (PL) were measured to investigate the luminescence characteristics of *m*-GaN. In addition, transmission electron microscopy (TEM) studies revealed that mixed partial dislocations (PDs) and basal stacking faults (BSFs) were threaded into the GaN layers.

3. Results and discussion

Fig. 2 shows the schematic diagrams and plan-view SEM and AFM images of the *m*-GaN grown with and without the SiN_x interlayer. The SEM images reveal smooth surface morphologies without pits or cracks in any of the samples. However, the AFM images show a rough surface with many small hillocks. The surface roughness (~10 nm) of *m*-GaN with the SiN_x interlayer slightly increased compared with that (~9 nm) of *m*-GaN without the SiN_x interlayer, which can be attributed to lateral growth on the SiN_x nano-masks.

Because the nanometer-sized hole in the SiN_x interlayer functions as a window in ELO, high-quality GaN with a low density of PDs and BSFs can be grown on the SiN_x interlayer.

Fig. 3(a) and (b) shows a schematic diagram describing the defect blocking mechanisms of the SiN_x interlayer and the cross-sectional SEM image of the SiN_x embedded in *m*-GaN, respectively. In previous research, it was reported that the SiN_x interlayer functioned as a defect-blocking layer [19,21]. Fig. 3(b) and (c) shows the existence of the SiN_x interlayer and the void (yellow circle) formation (void size below ~1 μm), indicating the lateral overgrowth over the SiN_x nano-mask layer.

The FWHMs of the DXRC were measured to compare the crystal qualities of samples with and without SiN_x interlayers, as shown in Fig. 4. The FWHMs of the (1 0 −1 0) peaks of the HVPE-grown 2-μm *m*-GaN template were 4399 and 1887 arcs, respectively, for scan

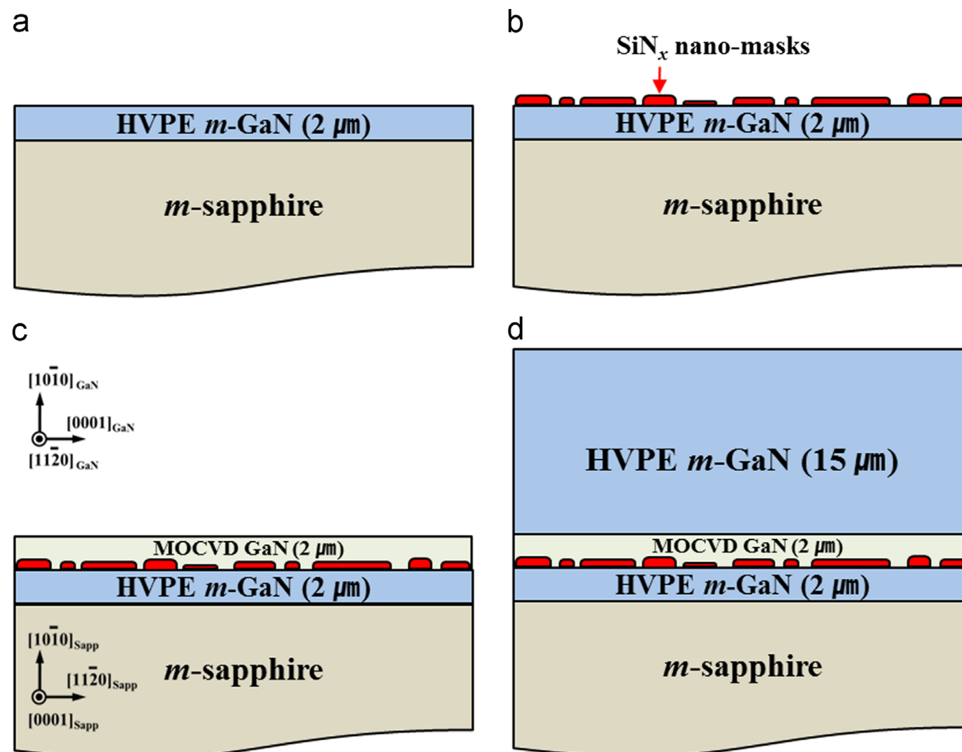

Fig. 1. Schematic diagrams of the experimental procedure: (a) *m*-GaN growth by HVPE, (b) SiN_x deposition by MOCVD, (c) GaN growth by MOCVD, and (d) thick GaN growth by HVPE.

Download English Version:

https://daneshyari.com/en/article/1790251

Download Persian Version:

https://daneshyari.com/article/1790251

Daneshyari.com